Regional modelling of rainfall erosivity:

Sensitivity of soil erosion to aerosol emissions

Authors: Hannah Nissan[1] and Ralf Toumi[1]

Running head:

Regional modelling of rainfall erosivity

Keywords:

Soil erosion, aerosols, climate model, regional climate modelling, indirect aerosol effects, precipitation, India, Bangladesh, Myanmar, South Asia

[1] Space & Atmospheric Physics Group, Blackett Laboratory, Imperial College London, UK.

Abstract

A rainfall erosivity scheme is implemented into the widely-used regional atmosphere-land model, WRF. Rainfall erosivity is parameterised from hourly precipitation and surface runoff in a high resolution (4 km) convection-permitting model. The scheme is used to examine the potential effects of changes in atmospheric aerosol concentrations on soil erosion in a case study of northern India and the surrounding countries for the 2010 monsoon season, using a model which isolates the indirect effect on cloud microphysics only. This study offers a preliminary investigation into this emerging topic, but longer simulations would be needed to establish a robust signal.

Summer precipitation is reduced in most areas and the monsoon circulation weakens for increases in cloud condensation nuclei concentrations. This can be attributed to localised cloud microphysical changes in the northeast of India, which induce a dynamic response opposing the monsoon circulation. The two regions of greatest decrease in erosion with increasing aerosol are in the Western Ghats and the Ganges Delta, both significant cropland areas. However, the effect is not uniform, with isolated local increases in soil erosion. These results suggest that, while efforts to reduce anthropogenic aerosol emissions may improve water availability for crops through enhanced rainfall, these benefits are likely to be tempered by an increase in soil erosion, though robust local changes were difficult to predict.

1. Introduction

The threat which soil erosion poses to sustainable food production worldwide has been largely underappreciated in public discourse and the scientific literature (Glatzel et al. 2014). Population growth is exerting increasing pressure on agricultural systems to provide enough food for all, and erosion is a serious threat to agricultural productivity (Pimentel et al. 1995; Yang et al. 2003).

Motivation to understand how soil erosion may evolve in a changing climate has led to the development of methods to use climate projections from global general circulation models

(GCMs) as input for erosion models. However, the disproportionate contribution of short, high intensity periods of rain to erosion necessitate hourly or higher frequency data in order to calculate rainfall erosivity, a key term in erosion modelling which expresses the potential of rain to cause erosion. Previous studies have used statistical methods to temporally and spatially downscale meteorological data from coarse GCM simulations to be used for erosion modelling.

Renard and Freimund (1994) developed empirical relations between rainfall erosivity and annual precipitation data in the United States. These were implemented by Nearing (2001) to calculate erosivity values from GCM projections. Others have used stochastic weather generators to produce rainfall data at the frequencies needed for hydrological impact models (Nicks & Gander 1994; Pruski & Nearing 2002b). To obtain local information from model data at low spatial resolutions, some have fitted transfer functions between GCM output and local rainfall observations (Zhang, 2005; Zhang, 2007; Zhang et al., 2010). Other studies have employed the 'change factor' method, applying relative shifts in precipitation between present and future simulations obtained from coarse climate model output directly to local baseline time series to infer likely local changes, without accounting for differences in climate variability across spatial scales (Pruski & Nearing 2002a; Hansen & Ines 2005; Favis-Mortlock & Guerra 1999).

In this study we implement a rainfall erosivity scheme in a regional climate model for the first time. This new approach permits simplistic soil erosion studies from an atmospheric science perspective, enabling dynamic investigations into the role of weather and climate in soil erosion on spatial scales where it is not practical to obtain data to parameterise erosion models. This method could be employed in regional climate change studies given sufficient computing resources. We use the new scheme to investigate how changes in aerosol emissions in the region around northern India may affect soil erosion via the regulation of rain and surface runoff production.

A complete understanding of the influence of aerosols on the environment, and subsequently on human and economic systems in South Asia remains elusive. While there is concern that current pollutant levels are damaging to public health, recent evidence suggests that the region has so far been shielded from the full effects of global warming by high aerosol concentrations (Menon et al. 2002). Emissions reduction measures could therefore lead to rapid warming, and subsequently to greater public health impacts from heat waves. At the same time, absorbing aerosols such as black are known to enhance glacial melt in the Himalaya, so lower emissions are likely to restrain the rate of global warming. Aerosol effects on monsoon precipitation are a major area of ongoing interest and research effort. In India, economic output from the agriculture industry ranks second in the world (Singh et al. 1992; Central Intelligence Agency 2013) and the timing and amount of the monsoon rains is of vital importance to agriculture, water security and the local economies (Li et al. 2015).

While much attention is focussed on how aerosols influence precipitation directly, there is less understanding of the potential impacts on downstream processes. Erosion directly affects food and water security, contaminates waterways and compromises agricultural productivity (UNEP 2007; Pimentel et al. 1995). As attempts are made to curb emissions of aerosol pollutants, policy makers should be informed about how these changes could affect a range of outcomes, including precipitation amount but also ecosystem services, agriculture and health. It might be anticipated that any change in erosion would mirror shifts in rainfall, but an idealised model study found that an increase in aerosol concentrations resulted in a change in rainfall erosivity which was amplified relative to the change in precipitation (Nissan and Toumi 2013b). Thus there is evidence to suggest that the agricultural impact of future measures to reduce emissions could be larger than anticipated.

This study presents the first attempt to assess the potential impacts of aerosols on soil erosion in South Asia. A thorough investigation of this question would involve a simulation over a period of decades, but for this sensitivity study computational constraints and the need to run the model at high temporal and spatial resolution limit us to only one monsoon season. Though no conclusions about the climatological influence of aerosols can be made from this, our results may be useful to inform fuller investigations into this important topic.

1.1. Modelling soil erosion

From an energy conservation perspective, erosion is a mechanical process for which the energy is provided by eroding agents. It may be wind or rain induced, but in most areas of the world rainfall driven erosion is the greater problem (Pimentel et al. 1995). Rain causes erosion by acting as an agent for the detachment and transport of eroded soils. The impact of raindrops on the ground, measured as the kinetic energy flux of the rain upon impact, provides the energy needed to overcome the friction binding sediment in the ground. Surface runoff (excess rain which is not absorbed by the land) must then be present to transport the detached sediment away. Raindrop impact and surface runoff are the most effective detachment and transport agents for erosion, and when these two drivers are combined substantial erosion can occur (Morgan 1986). Other factors such as slope, vegetation cover, farming practices and soil type also influence the amount of erosion that takes place, and there are many erosion models which incorporate these factors. Most include considerable detail on soil processes, while employing simplistic treatments of rainfall, and require input data at high temporal and spatial resolutions.

The Universal Soil Loss Equation (USLE, Wischmeier and Smith 1978) and its revised version, the RUSLE (Renard et al. 1997), are the most widely used erosion models in the world. Both estimate interill erosion, caused by raindrops striking soil directly, as opposed to by tiny streams (rills) or river erosion. As relatively simple empirical tools, they require fewer data than more sophisticated alternatives, and can be employed over large regions because computational constraints are not a problem. Rainfall erosivity, *R,* is a key term in the USLE/RUSLE, encapsulating both sediment detachment and transport processes. The original USLE/RUSLE erosivity parameter was widely criticised for its failure to incorporate surface runoff, using maximum rainfall intensity instead as a proxy for the production of runoff. With this in mind, Kinnell et al. (1994) proposed an alternative formulation for erosivity, which they found superior on comparison with observations of erosion in Mississippi:

$$R = \sum_{t} q_t e_t (\Delta t)^2 \tag{1}$$

where q_t and e_t are the runoff rate and rainfall kinetic energy flux at time t, occurring over duration Δt.

Total rainfall kinetic energy flux is parameterised from hourly rainfall intensity according to either a logarithmic (Wischmeier & Smith 1958) or exponential (Brown & Foster 1987) formulation. Intensity data is needed at this high temporal resolution because of the cubic dependence of e_t on raindrop speed, which itself is positively correlated with intensity. Aggregating rainfall data across longer durations would underestimate the contribution of heavy rainfall periods, which contribute disproportionately to the total rainfall erosivity. Here we model hourly precipitation and surface runoff at a significantly higher temporal and spatial resolution, allowing us to estimate rainfall driven soil erosion.

1.2. Aerosols, the monsoon and soil erosion

We also contribute to the existing literature on the influence of aerosols on the South Asian monsoon. Modelling studies have shown that the decreasing trend in monsoon precipitation observed over the last half of the twentieth century (Turner and Annamalai 2012) is due in part to rising aerosol emissions (Guo et al. 2014; Bollasina et al. 2011). This opposes the influence of increasing greenhouse gas emissions, which would otherwise enhance precipitation in the region, as the thermal land-sea contrast is enhanced and moisture transport increases from the warming Indian Ocean (Turner and Annamalai 2012; Li et al. 2015).

Scattering aerosols (primarily sulphates) cool the surface by blocking solar radiation. As the sources of these aerosols are mainly over land, this heterogeneous spatial cooling pattern reduces the meridional thermal contrast which drives the monsoon circulation. Sea surface temperatures can also decrease, limiting the transport of moisture flux from the Indian Ocean and lowering precipitation (Turner and Annamalai 2012). Aerosols also interact with the hydrological system in a number of 'indirect' ways via their role as condensation nuclei in the formation of clouds. For a given cloud water content, increased concentrations of aerosols cause this water to be shared among a greater number of smaller droplets, increasing cloud albedo, cloud lifetime and suppressing precipitation. Recent studies suggest that these indirect effects are the dominant regulator of monsoon precipitation (Bollasina et al. 2011; Guo et al. 2014). However, there is disagreement about the role absorbing aerosols such as black carbon and dust (Turner and Annamalai 2012; Ramanathan et al. 2005; Lau and Kim 2006; Lau et al. 2006).

Where most previous aerosol studies have used General Circulation Models (GCMs) or regional models run at coarse spatial resolutions, we use a regional atmospheric model run at 4 km grid spacing. This convection-permitting setup resolves key features of the landscape, such as the Western Ghats and the Himalaya, which are poorly represented by GCMs. However, the computational expense limits us to the only one monsoon season so our results must be set in the context of other work. We also address a research gap concerning the nature of aerosol indirect effects in climate models and their influence on monsoon precipitation specifically (Guo et al. 2014). We use a model which isolates the indirect aerosol effects only; while most earlier work has inferred the influence of indirect aerosol effects on the monsoon and precipitation, we are able to examine these processes explicitly, albeit for this short period.

2. Methods

2.1. Model setup

We used the Weather Research and Forecasting model (WRF version 3.6, Skamarock et al. 2008) to simulate one monsoon season (June to September, JJAS) in 2010 for our sensitivity study. WRF is widely used and has been implemented extensively to model the climate and weather of India (e.g. Srinivas et al. 2013). Three domain nests were set up with one way nesting at 36km, 12km and 4km grid spacing, and 45 vertical levels between the ground and the model top at 500 hPa (Figure 1). The outer model domain was chosen to include the main features of the monsoon circulation. The inner domain captures the most erosive parts of India

(Narayana, 1984) while restricting the size of the nest to limit computational expense. The positioning of the domain boundaries was tested to ensure model stability given the complex topography in the region.

The computational cost of running at this resolution prohibited a longer simulation over a wider region and multiple years. This was a necessary compromise. Since the model aerosol parameterisation is linked only with the microphysics, not the convective scheme, a convection-permitting resolution was required. Moreover, hourly rainfall data are needed for the simulation of erosivity. Fluctuations at this frequency occur on small spatial scales, so a relatively high spatial resolution was needed.

The new 'aerosol-aware' microphysics scheme (Thompson & Eidhammer 2014) was selected and is described in further detail below. The Kain-Fritsch convective scheme was used in the outer two domains (Kain 2004) and boundary layer parameterisation followed Hong et al. (2006), while the short- and long-wave RRTM radiation schemes followed Mlawer et al. (1997). The atmospheric surface layer was modelled with Monin-Obukhov similarity theory and the land surface with the unified NOAH land surface model (Chen & Dudhia 2001). This setup includes the most commonly used WRF parameterisations used for modelling India (based on a literature review using the keywords 'India' and 'WRF').

ERA Interim reanalysis data were used to provide lateral boundary conditions for the outer domain only and sea surface temperatures for all model domains at six-hourly intervals. The outer 5 grid boxes of each domain were excluded from the analysis to remove the influence of boundary conditions. The 2010 monsoon season was a fairly typical season in the ERA Interim record, with average near surface temperature, wind speed and precipitation within one standard deviation of the long term (1978-2014) average in the region of interest. The intra-seasonal variability (standard deviation of the 5-day running mean) was within one standard deviation of the long term average for wind speed and precipitation, though intra-seasonal near surface temperature variability was below the long term average.

2.2. Parameterisation of indirect aerosol effects

We used the new 'aerosol-aware' bulk microphysics parameterisation (Thompson & Eidhammer 2014). The scheme models five water species: cloud water, rain, cloud ice, snow and graupel. It is double moment in cloud water, cloud ice and rain, predicting both mass mixing ratio and number concentration for these hydrometeor species, and single moment in snow and graupel. For the single moment hydrometeors, only the mass is prognosed, and the number concentrations can be diagnosed from an assumed gamma particle size distribution. The number concentrations of two bulk aerosol categories, cloud condensation nuclei (CCN) and ice nuclei (IN, which includes only dust), are also simulated. Cloud droplets and ice particles are then nucleated onto these particles.

Based on a global, spatially heterogeneous climatology of aerosol concentrations (Figure 1), the scheme estimates surface emissions according to a simple parameterisation applied only to the lowest model level, which assumes that local emissions are greatest where the atmospheric loading is high:

$$\frac{dN_{WFA}}{dt} = 10^{[\log[N_{WFA}]-3.699]} \times h \tag{2}$$

where N_{WFA} is the number concentration of 'water-friendly aerosols' (CCN) and h is a scaling factor given by

$$h = 0.875 + 0.125\left[\frac{20000-\sqrt{dxdy}}{16000}\right]\times\frac{\sqrt{dxdy}}{20000} \qquad \text{for } \frac{\sqrt{dxdy}}{20000} < 1$$

(3)

$$h = 0.875 \qquad \text{for } \frac{\sqrt{dxdy}}{20000} \geq 1$$

In Eq. (3), dx and dy are the resolution in the longitudinal and latitudinal directions, respectively. These emissions are then added to the background aerosol concentrations during the simulation. These background concentrations are derived from global aerosol simulations during 2001-7 using the GOCART model (Ginoux et al. 2001; Chin, Rood, et al. 2000a; Chin, Savoie, et al. 2000b), a bin resolving aerosol model which includes natural and anthropogenic sources of several different types of aerosols and their precursors. The aerosol inputs used by the microphysics scheme include mixing ratios of sulphates, sea salts, organic carbon, dust and black carbon. The model categorises these into water (CCN) and ice (IN) friendly aerosols based on their size: dust aerosols greater than 0.5μm are treated as IN, while all remaining aerosols except black carbon are assumed to be CCN.

This setup exclusively models the 'indirect' aerosol effects on clouds and precipitation, and omits the 'direct' effects of aerosols on radiation, since aerosol optical depth is not communicated to the model radiation scheme. However, dynamic responses to changes in cloud properties and precipitation processes are captured via effective cloud droplet and ice particle sizes, which are relayed to the radiation scheme.

2.3. Sensitivity Studies

We performed several sensitivity studies. The rate of aerosol emissions was changed by multiplying and dividing the scaling factor, h, in Eq. (**2)** by a factor of 10 to represent a tenfold increase and decrease in the rate of emissions. The three model simulations will be referred to as LOW (emissions rate divided by 10), CTL (default emissions rate) and HIGH (emissions rate multiplied by 10). This resulted in average concentrations of 385, 1057 and 2360 CCN cm^{-3} and 2.22, 2.17 and 2.30 IN cm^{-3} in emissions scenarios LOW, CTL and HIGH, respectively, in agreement with the range in previous aerosol sensitivity studies (Fan et al. 2012).

Kinetic energy flux, e, was parameterised offline from hourly model rainfall intensity, i, using the empirical relationship given by Brown and Foster (1987), recommended in the RUSLE, and verified by Nissan and Toumi (2013a):

$$e = 29i[1 - 0.72exp^{-0.05i}] \quad (4)$$

Total JJAS rainfall erosivity was calculated according to Eq. (**1)**, and used to estimate erosion from the regressions between soil loss and rainfall erosivity published by Kinnell et al. (1994):

$$A = 4.27\times10^{-3}R \quad (5)$$

with R in Jm^{-1} and A in T/A. Equation (**5)** was only available from soil loss and erosivity data for storms over a five year period on a plot in Mississippi, but this is adequate for the sensitivity study. We assume that other factors such as soil type, slope and crop management practices remain constant throughout the different aerosol experiments, as in other studies, to give a first order approximation of the change in erosion rates (Narayana 1984).

3. Results

3.1. Comparison with observations

The monsoon circulation is illustrated in Figure 2a. During the summer months, moisture is advected by westerly winds from the Arabian Sea, which turn south-westerly in the Bay of Bengal. Precipitation falls mainly in the most mountainous areas: the Western Ghats along the west coast of the country and in the north east of the domain (the foothills of the Himalaya, the Ganges Delta and Myanmar). The 4km model captures both the spatial pattern and the amount of precipitation significantly better than the 36km nest, which shows very little rain throughout the domain (Figures 2b & 3c). The resolution of the TRMM rain gauge observations is coarser than 4km, but it can be seen that the higher resolution model successfully represents rainfall maxima along the Western Ghats and in the foothills of the Himalaya, and significant offshore rainfall over the Bay of Bengal and off the west coast of India. However, it underestimates the lighter rainfall observed over the rest of the domain, in particular over northwest India and in the western part of the Bay of Bengal.

This dry bias over South Asia is a persistent problem in climate models. The multi-model mean relative error of the CMIP-5 ensemble of GCMs compared with precipitation analyses from the Global Precipitation Climatology Project (GPCP) shows a bias of between -15% and -45% over India (Flato et al. 2013). ERA winds appear to be low over central India, offering a possible explanation for the dry bias in this region (Figure 2a). The daily rainfall time series (Figure 3) shows that the model rainfall approaches the observations at higher resolution, with a sharp increase in rain between the 12km and 4km nests. This is likely due to the convective scheme in the outer two nests, which is not used at 4km.

The maximum in the foothills of the Himalaya is higher in the model than in the observations, which could be due to the enhanced spatial resolution of the model; the observations are smoothed by interpolation to 0.5° resolution, which will reduce the magnitude of local high values. Comparing the outer- and inner-most model nests confirms that this localised high rainfall is attributable to higher resolution in the 4km nest (Figure 2).

3.2. Influence of aerosol indirect effects on the 2010 monsoon

Although not the main purpose of this work it is instructive to evaluate the impact of increasing aerosol emissions on the general monsoon circulation during this sample year.

The model simulates a weakening of the monsoon circulation with increasing aerosols, with anomalous winds blowing counter to the prevailing circulation (Figures 2a & 4a). An anomalous high pressure anticyclone is present in the high aerosol experiment (HIGH) in the region of the Ganges Delta, which develops early in the simulation (Figures 4a & 4b). This is consistent with earlier work by Guo et al. (2014) and Bollasina et al. (2011), though these studies did not identify a similar high pressure anticyclone. Among twenty-five CMIP-5 GCMs, Guo et al. (2014) found that models which include both direct and indirect aerosol effects as well as greenhouse gas (GHG) increases show no significant change in moisture flux in South Asia, while those with only direct aerosol effects and GHGs show an intensification of the monsoon circulation. We infer from this that our study of just one year is consistent with previous work in that the indirect effects of aerosols induce a dynamic response opposing the regional circulation, but that this is masked by the amplifying effect of the rise in GHG concentrations in those studies. Our simulations do not include any change in GHG emissions, so a weakening monsoon circulation is in agreement with the behaviour of the CMIP-5 models. The fact that we find similar behaviour using a different (regional) model lends support to this finding.

In agreement with other modelling studies (Chung and Ramanathan 2006; Bollasina et al. 2011), increasing aerosol emissions leads to drying in most regions of the model domain (Figure 5b). We find an 18% decrease in total precipitation across the domain between the lowest and highest aerosol simulations. In attributing this to the rise in aerosol emissions, we assume that the dry model bias is independent of the aerosol load. Notable precipitation decreases occur in the areas of greatest rainfall, along the Western Ghats, the foothills of the Himalaya and Bangladesh, and on the west coast of Myanmar. Localised precipitation increases occur in the central-north and north-east of the domain (Figure 5a). This is not seen in other modelling studies using GCMs (Guo et al. 2014; Bollasina et al. 2011), and we postulate that it could be the result of higher spatial resolution in our model in this very mountainous area. The feature is also present in the 36km nest (not shown) but this scale is still finer than the resolution of the CMIP5 models. The pattern of the increase in rain in this region is also consistent with the anomalous anticyclonic circulation (Figure 4a), which diverts moisture, normally arriving in Bangladesh from the Bay of Bengal, towards the west, and closes the circulation loop further north, where another band of increased rainfall can be seen in Figure 5a.

The footprint of the rainfall change is also surprisingly similar to the observed pattern of change in monsoon rainfall since 1950, a period which has seen substantial increases in aerosol concentrations in South Asia (Turner and Annamalai, 2012). While these cannot be compared directly given the limited scope of our model setup, this nevertheless suggests that some of the key processes for regulating the long term trend in monsoon precipitation since 1950 may be represented by our short sensitivity study.

To consider how including direct aerosol effects in our model might influence our results, we refer to Guo et al (2014). In GCMs with both indirect and direct effects, rainfall increased in western and southern India, with drying in the north and east of the domain as in our study. We therefore would not expect a change to the signal in the Ganges Delta with direct effects, but it is possible that the drying signal found in the Ghats in our study would be reversed because direct effects tend to strengthen the monsoon circulation. However, as models with only indirect effects also did not discern this feature it is difficult to determine. With one-way nesting, our experiment cannot capture the influence of local effects on the wider circulation in the region, but we speculate that two way nesting is unlikely to alter our main conclusions since the changes in temperature and low level winds in the outer domain are in the same direction as, but smaller in magnitude than the inner nest.

Confidence intervals for the change in mean daily rain were computed using bias-corrected bootstrap sampling with 1000 samples. This showed wide confidence intervals over much of the domain, spanning positive and negative changes in some areas. However, when aggregated over the whole domain and over the two areas of most significant change, the Western Ghats and the Ganges Delta, the confidence intervals are narrow with negative upper limits for all three areas. A larger spatial scale is needed to detect the change because of the redistribution of rainfall within the domain and the short time series available. Longer simulations may allow a clearer signal to emerge at the local level.

The top of atmosphere albedo reflects changes in cloud properties brought about by the rise in aerosol emissions. Figure 4c shows a widespread increase in albedo in the first two months of the monsoon season. Over land, it is the already rainy areas that also see the greatest increase. A decrease in average cloud droplet size from 0.16 mm to 0.11 mm between the LOW and HIGH simulations can lead to prolonged cloud lifetime and an increase in cloud albedo, reducing surface insolation. This is particularly notable in the northeast of the domain (Figure 4c).

We therefore identify both local aerosol-cloud effects and dynamic circulation changes in the model. The increase in aerosol emissions is greatest in the northeast, where background concentrations are highest (Eq. (**2)**, Figure 1). The effect of this on local cloud microphysical structure during the early part of the summer enhances cloud albedo and causes surface cooling (-0.1C on average and up to -0.7C in the north-east) and high pressure in the region, driving an anomalous anticyclonic flow that continues throughout the rainy season (Figure 4). This extends across a large portion of the model domain, weakening the prevailing monsoon dynamic. It also reduces the thermal land-sea contrast, weakening the meridional overturning circulation to compensate for the energy imbalance (Bollasina et al. 2011).

In contrast with Guo et al. (2014), who propose that precipitation is suppressed wholly by local aerosol-cloud interactions in an ensemble of CMIP-5 models (Squires & Twomey 1960; Albrecht 1989), we suggest that (in our model setup) it is this weaker circulation that leads to reduced precipitation because the drying can be clearly seen in the Ghats, far from the main source of the emissions (Figure 1, Figure 5b). The topography of the Ghats is poorly resolved in most GCMs, and this effect was not seen in that study, nor in the NOAA GFDL model (Bollasina et al. 2011). In an analysis of thirty five CMIP-5 models interpolated to a higher resolution than these studies, Li et al. (2015) did observe drying in the Ghats in the historical twentieth century simulations. Consistent with our findings, Li et al. (2015) concluded that aerosol-induced dynamic circulation changes were the dominant control on monsoon rainfall in the twentieth century, though they made no distinction between direct and indirect aerosol effects. Furthermore, the distribution of hourly rainfall intensity for the whole season (and for separate months, not shown) is largely unchanged between the low and high aerosol experiments, both across the domain and in the Ganges Delta region (Figure 6a and 6d). If precipitation were suppressed by local aerosol interactions, we would expect to see a reduction in the lowest quantiles of rainfall intensity, as smaller cloud droplets inhibit the collision and coalescence processes that lead to rain formation. Since there are localised increases and decreases in the north-east, the change in distribution for a subset of the Ganges Delta area with entirely negative change in mean precipitation was also investigated, but no reduction in the lower quantiles was found, for any month. The similarity in the rainfall distributions suggests that the same physical processes are at work in each simulation, and the drying can instead be explained by an 18% average reduction in the number of rainy days, consistent with a primarily dynamic response to the aerosol forcing.

3.3. Influence of aerosols on the land surface

We examine the effect of aerosols on soil moisture and surface runoff, both important factors in determining soil erosion. As expected, the spatial patterns of daily mean soil moisture and surface runoff follow the precipitation field (Figure 7a,b and Figure 2). Precipitation falling at the surface is either evaporated, absorbed by the soil, or becomes surface runoff. Neglecting evaporation, which is slow to respond, we expect changes in precipitation to be largely balanced by local changes in soil moisture and runoff. This is confirmed by Figures 7c and 7d. The direction of change of both variables mirrors the precipitation change seen in Figure 5. The largest changes in runoff occur in the east & north-east of the domain and over the Western Ghats, while the greatest soil moisture changes appear in central-northern India and Myanmar. In regions of steep topography, rainfall is less easily absorbed into the soil and runoff is quickly produced. Conversely, where the ground is flatter, in central-northern India, runoff is less easily produced and changes in rainfall translate more readily into drying or moistening of the land surface. The decrease in soil moisture in the northern Ghats and the increase in Myanmar are exceptions to this general pattern.

The very high temporal resolution of the model data allows us to examine the behaviour of hourly extremes, which strongly influence erosion rates. Despite the rainfall intensity distribution being largely unaffected by the increase in aerosol emissions, the upper quantiles of hourly surface runoff are lower in the high aerosol simulation (Figure 6b). The largest decrease in extreme hourly runoff rate occurs in northeast India and the Ganges Delta region (Figure 8d). This collocates well with the decrease in extreme rainfall intensity (Figure 8c) and the general drying of soil in that area (Figure 7c). However, the reduction in extreme precipitation is offset by increases elsewhere in the domain, so we do not observe a similar change in the upper end of the intensity distribution (Figure 6a).

3.4. Aerosol effects on soil erosion

The level of temporal detail captured by the model can be seen in the time series shown in Figure 9. Sub-storm fluctuations of precipitation intensity and runoff are discerned by the model, allowing for a more physical estimation of rainfall erosivity than is permitted by aggregated rainfall data which are typically available. Rain intensity and runoff in the most polluted aerosol experiment closely mirror the cleaner simulation when averaged over the domain (Figures 9a and 9b). This was not the case for smaller areas, confirming that the increased aerosol emissions led to a spatial redistribution of rainfall.

Figure 9c compares time series of domain-averaged rain intensity and two measures of erosivity: R (Eq. (**1**)) and R_{EI}, which was calculated using intensity as a proxy for surface runoff in Eq. (**1**), as runoff data are often unavailable (Kinnell 2010). R_{EI} is consistently higher than R, suggesting that measures of erosivity which use rain as a proxy for runoff as the transport agent in the erosive process are likely to overestimate erosion rates. This assumes that all rain produces overland flow, while in reality the fraction of precipitation that goes into runoff is considerably less and this fraction is not constant.

The distribution of grid total erosivity mirrors runoff, predominantly showing decreases in the most erosive areas (Figure 10a,b Figure 7b,d). As with precipitation, local changes in mean daily erosivity had large confidence intervals, spanning positive and negative changes in some places, but the aggregated change over the whole domain, the Ganges Delta and the Western Ghats showed a robust decrease in all three areas. The spatial pattern of estimated soil erosion, (Figure 10c, from Eq. 5), follows that of precipitation (Figure 2c) and rainfall erosivity (Figure 10a). Narayana (1984) estimated the total soil erosion in India to be 5,334 million tonnes, based on rainfall and runoff data, of which 3,282 million tonnes was due to interill erosion (as opposed to river and rill erosion). Total estimated interill erosion in our smaller domain was only 677 million tonnes in the CTL control simulation. The difference may be largely explained by the dry bias in model precipitation, and the smaller domain used in this research. Both studies give only rough first order approximations of erosion rates, making simplifying assumptions for other factors such as slope, crop management practices and soil type.

Figure 10d shows the change in total erosion between the lowest and highest aerosol loading experiments. In areas of steep topography, where changes in precipitation are reflected primarily in runoff changes, erosion is also seen to follow the pattern of rainfall change. In less steep regions with low erosion rates, such as in central-northern India, where precipitation increases lead to higher soil moisture and not to increased runoff (Figure 7), there is little change in erosion.

We identify two principal erosive regions: the area around the Ganges Delta and the Western Ghats, and focus our analysis on these areas (Figures 10e and 10f). This is consistent with Narayana (1984), whose estimates of soil erosion revealed that the Himalayan foothills were the second most erosive area in the country, after rill erosion occurring along the banks of rivers in Gujarat. The lack of substantial model erosion in Gujarat likely stems from the underestimation of precipitation in this area (Figure 2), and the fact that we consider only interill erosion. Singh et al. (1992) estimated erosion using the Universal Soil Loss Equation and also found high rates in the Western Ghats.

Land use in these regions is mixed, but both contain substantial areas of cropland (National Land Cover Database (Homer et al 2004)). The Ganges Delta consists mainly of forests and crops, while the Western Ghats is a mixture of trees and shrubbery with crops slightly inland. Increased aerosol loading causes a reduction in estimated soil erosion in both areas, with localised increases following the precipitation pattern.

We do not find an amplified sensitivity of total JJAS soil erosion to aerosols compared with the precipitation response, as was suggested by earlier idealised simulations of convective and orographic rainfall (Nissan and Toumi 2013b). At the hourly level, the definition of rainfall erosivity as the product of two positively correlated variables, rainfall kinetic energy flux and surface runoff rate (Eq. (1**)**, means that any change in rainfall erosivity must be larger than the change in either of these variables. However, the summer monsoon season consists of many separate rainy episodes, which may become more or less intense in the polluted simulation. Changing dynamics mean that some weather patterns present in the clean LOW simulation are not in the polluted HIGH run and vice versa, or are shifted in time or space. The change in the total rainfall erosivity is the sum of the contributions from each of these rainy periods. For an isolated storm we continue to expect clearer amplification of the aerosol effect on soil erosion, compared with the change in precipitation.

4. Conclusion

Motivated by earlier work suggesting that aerosols may affect soil erosion in a manner which is not obvious from the pattern of precipitation change, we implemented a rainfall erosivity scheme into the widely-used WRF regional model. Surface runoff data are needed to model soil erosion but are often unavailable at the required space and time resolutions. The new methodology uses hourly precipitation and runoff to parameterise rainfall erosivity using runoff modelled by the NOAH land surface scheme within WRF. This high frequency is needed because of the nonlinear dependence of rainfall erosivity on precipitation intensity. Storm- or season-aggregated data forgo valuable information about the high intensities reached within storms, which have a disproportionate influence on rainfall erosivity compared with their frequency of occurrence. Due to the unavailability of runoff data, alternative erosivity parameters use rain intensity as a proxy for surface runoff to represent the transport agent in the erosive process, but our results suggest these may result in an overestimation of soil erosion.

We present a sensitivity study examining the potential effects of increasing aerosol emissions on soil erosion during the 2010 monsoon season (June to September) in a domain centred on northern India. This region is strongly dependent on agriculture and already suffers from extensive and severe land degradation (Singh et al. 1992). The model was run at a convection-permitting spatial resolution of 4km, using ERA-Interim reanalysis data for the model boundary conditions. Using the new aerosol-microphysics WRF parameterisation scheme, which includes the indirect effects of aerosols on clouds and precipitation only, we performed three simulations with increasing rates of aerosol emissions.

We found that increasing aerosol emissions led to a drying over much of the domain (-18%). Localised increases in precipitation were also found, unlike in previous modelling studies using coarser resolution GCMs. Aggregating over the season and over parts of the domain allowed a strong signal to emerge, but a longer time series would be needed to detect robust changes in rainfall and erosivity at the local grid level. We attribute the drying in our model to a combination of localised aerosol-cloud interactions in northeast India and subsequent dynamic changes which weaken the monsoon circulation. The strong drying signal in the Ghats, far from the source of aerosol emissions, is the fingerprint of this dynamic response to aerosols in the model.

Results indicated two main erosive areas, collocated with the heaviest precipitation and surface runoff: the Western Ghats and the northeast of the domain in the foothills of the Himalaya and the Ganges Delta. Other regions of substantial soil erosion were likely underestimated due to the dry precipitation bias in parts of India in the model. As aerosol emissions increased, estimated soil erosion decreased in both regions, with localised increases in erosion following the precipitation change. Our results indicate that, while plans to reduce emissions may improve water supply for crops through enhanced rainfall in most areas, this benefit could be tempered by increased soil erosion. However, we also found localised areas of positive rainfall and erosion sensitivity to aerosols. In these areas, emissions reduction could adversely impact upon agriculture through decreased rainfall, but this negative effect may be cushioned by a reduction in the rate of soil erosion.

We caution that these results pertain to one monsoon season only, and that our model includes no changes in greenhouse gas and no direct aerosol effects. The principal limitation of the methodology presented is the need for high resolution. Longer simulations would be needed to determine the true sensitivity of erosivity to aerosol emissions, but computational constraints are prohibitive at this time.

Figure captions

Figure 1: Concentrations of cloud condensation nuclei (kg^{-1}) in the climatology of aerosol concentrations used for the CTL simulation, based on the GOCART model from 2001-7 (Thompson & Eidhammer 2014). The three model nests are also shown, with 36km, 12km and 4km resolution from the largest (full picture) to smallest (inner box) domain.

Figure 2: Average daily precipitation (contours, mm) and 10m wind (vectors) from a) TRMM satellite precipitation observations and ERA Interim winds, b) 36km and c) 4km WRF CTL simulations. The spatial pattern of the modelled precipitation is similar in the LOW and HIGH WRF simulations.

Figure 3: Time series of domain-averaged daily observed precipitation (mm) from TRMM, and WRF 36km, 12km and 4km modelled precipitation in the CTL simulation.

Figure 4: Change in JJAS a) average moisture flux integrated between 950 and 750hPa ($kgm^{-1}s^{-1}$). Positive (negative) fluxes are shown by forward (backward) hatching in regions with greater than ±10 $kgm^{-1}s^{-1}$ difference. Change in June and July (JJ) b) average surface pressure (Pa) and d) top of atmosphere albedo between the LOW and HIGH simulations. In b) and c) contours are positive with negative areas indicated by hatching; in d) only changes greater than ±0.01 are shown.

Figure 5: Change in average daily precipitation (mm), split into a) negative and b) positive changes.

Figure 6: Quantile - quantile plot comparing the domain-wide distributions of hourly a) rainfall intensity (mmh^{-1}) b) runoff rate (mmh^{-1}) and c) erosivity R_{EQ} (Jm^{-1}) and d) hourly rainfall intensity in a region of negative mean rainfall change in the Ganges Delta area, between the LOW and HIGH simulations. The horizontal (vertical) axis shows the quantiles of the lowest (highest) aerosol experiment. The one-to-one line is also shown: two similar distributions would lie close to this line.

Figure 7: a) Mean soil moisture (m^3m^{-3}) and b) daily mean surface runoff (mm) in the LOW simulation. Change in c) mean soil moisture (m^3m^{-3}) greater than ±0.05 m^3m^{-3} and d) daily mean surface runoff (mm) greater than ±1 mm between the LOW and HIGH simulations. Contours are positive in c), and areas of negative change are indicated by hatching. In d) contours are negative while hatching indictaes positive change.

Figure 8: 99th percentile of hourly a) rainfall intensity (mmh^{-1}) and b) surface runoff rate (mmh^{-1}) in the LOW simulation. Change in the 99th percentile of hourly c) rainfall intensity (mmh^{-1}) and d) surface runoff rate (mmh^{-1}) between the LOW and HIGH simulations. In c) and d) contours are negative and hatching shows areas of positive change, with only changes greater than ±0.05 mmh^{-1} indicated.

Figure 9: Time series of domain-wide average a) rainfall intensity (mmh^{-1}) and b) surface runoff rate (mmh^{-1}) in the simulations with the lowest (LOW, black line) and highest (HIGH, grey line) aerosol loadings, shown for the first 60 days. c) Time series of domain-wide average rainfall intensity (mmh^{-1}, black solid line, left axis), rainfall erosivity R_{EQ} (Jm^{-1}, black dotted line, middle axis) and rainfall erosivity R_{EI} (Jm^{-1}, grey line, right axis) in the LOW simulation, shown for 20 days for clarity. Intensity was used as a proxy for surface runoff in Eq. (1) to calculate R_{EI}.

Figure 10: JJAS total a) rainfall erosivity R_{EQ} (Jm^{-1}) and c) estimated soil erosion (T/A) in the LOW simulation. b) Change in JJAS total rainfall erosivity R_{EQ} (Jm^{-1}) greater than ±50 Jm^{-1} and d) JJAS total estimated soil erosion (T/A) greater than ±0.25 T/A between the LOW and HIGH simulations. Percentage change greater than ±10% in JJAS total estimated soil erosion in e) the Ganges Delta and f) the Western Ghats regions between the LOW and HIGH simulations. In e) and f) grids with estimated total erosion less than 2 T/A have been excluded from the calculation. In b), d), e) and f), contours are negative and hatching shows areas of positive change.

References

Albrecht, B.A., 1989. Aerosols, cloud microphysics, and fractional cloudiness. *Science*, 245(4923), pp.1227–1230.

Bollasina, M. a., Ming, Y. & Ramaswamy, V., 2011. Anthropogenic Aerosols and the Weakening of the South Asian Summer Monsoon. *Science*, 334(6055), pp.502–505.

Brown, L.C. & Foster, G.R., 1987. Storm erosivity using idealized intensity distributions. *Transactions of the ASABE*, 30(2), pp.0379 –0386.

Central Intelligence Agency, 2013. *The World Factbook 2013-14*, Washington, |DC.

Chen, F. & Dudhia, J., 2001. Coupling an advanced land surface-hydrology model with the Penn State-NCAR MM5 modeling system. Part I: model implementation and sensitivity. *Monthly Weather Review*, 129(4), pp.569–585.

Chin, M., Savoie, D.L., et al., 2000. Atmospheric sulfur cycle simulated in the global model GOCART: Comparison with field observations and regional budgets. *Journal of geophysical research*, 105(D20).

Chin, M., Rood, R.B., et al., 2000. Atmospheric sulfur cycle simulated in the global model GOCART: Model description and global properties.

Chung, C.E. & Ramanathan, V., 2006. Weakening of north Indian SST gradients and the monsoon rainfall in India and the Sahel. *Journal of Climate*, 19(10), pp.2036–2045.

Fan, J. et al., 2012. Aerosol impacts on clouds and precipitation in eastern China: results from bin and bulk microphysics. *Journal of Geophysical Research*, 117, pp.1–21.

Favis-Mortlock, D.T. & Guerra, A.J.., 1999. The implications of general circulation model estimates of rainfall for future erosion: a case study from Brazil. *Catena*, 37(3-4), pp.329–354.

Flato, G. et al., 2013. Evaluation of Climate Models. In T. F. Stocker et al., eds. *Climate Change 2013: The Physical Science Basis. Contribution of Working Group I to the Fifth Assessment Report of the Intergovernmental Panel on Climate Change*. Cambridge University Press, Cambridge, United Kingdom and New York, NY, USA.

Ginoux, P. et al., 2001. Sources and distributions of dust aerosols simulated with the GOCART model. *Journal of Geophysical Research: Atmospheres*, 106(D17), pp.20255–20273. Available at: http://dx.doi.org/10.1029/2000JD000053.

Glatzel, K. et al., 2014. *No ordinary matter: conserving, restoring and enhancing Africa's soils*,

Guo, L., Turner, A. & Highwood, E., 2014. Impacts of 20th century aerosol emissions on the South Asian monsoon in the CMIP5 models. *Atmospheric Chemistry and Physics*, 14, pp.30639–30666.

Hansen, J.W. & Ines, A.V.M., 2005. Stochastic disaggregation of monthly rainfall data for crop simulation studies. *Agricultural and Forest Meteorology*, 131, pp.233–246.

Hong, S.-Y., Noh, Y. & Dudhia, J., 2006. A new vertical diffusion package with an explicit treatment of entrainment processes. *Monthly Weather Review*, 134(9), pp.2318–2341.

Kain, J.S., 2004. The Kain-Fritsch convective parameterization: an update. *Journal of Applied Meteorology*, 43(1), pp.170–181.

Kinnell, P.I.A., 2010. Event soil loss, runoff and the Universal Soil Loss Equation family of models: A review. *Journal of Hydrology*, 385, pp.384–397.

Kinnell, P.I.A., McGregor, K.C. & Rosewell, C.J., 1994. The IXEA index as an alternative to the EI30 erosivity index. *Transactions of the American Society of Agricultural Engineers*, 37(5), pp.1449–1456.

Lau, K.M. & Kim, K.M., 2006. Observational relationships between aerosol and Asian monsoon rainfall, and circulation. *Geophysical Research Letters*, 33(21), pp.1–5.

Lau, K.M., Kim, M.K. & Kim, K.M., 2006. Asian summer monsoon anomalies induced by aerosol direct forcing: The role of the Tibetan Plateau. *Climate Dynamics*, 26(7-8), pp.855–864.

Li, X. et al., 2015. Mechanisms of Asian Summer Monsoon Changes in Response to Anthropogenic Forcing in CMIP5 Models. *Journal of Climate*, p.150319112745003. Available at: http://journals.ametsoc.org/doi/abs/10.1175/JCLI-D-14-00559.1.

Menon, S. et al., 2002. Climate effects of black carbon aerosols in China and India. *Science (New York, N.Y.)*, 297(5590), pp.2250–3. Available at: http://www.ncbi.nlm.nih.gov/pubmed/12351786 [Accessed July 4, 2016].

Mlawer, E.J. et al., 1997. Radiative transfer for inhomogeneous atmospheres: RRTM, a validated correlated-k model for the longwave. *Journal of Geophysical Research*, 102.

Morgan, R.P.C., 1986. *Soil Erosion and Conservation* Second., Longman Group UK Limited.

Narayana, D.V. V., 1984. Estimation of soil erosion in india. *Journal of Irrigation and Drainage Engineering*, 109(4), pp.419–434.

Nearing, M.A., 2001. Potential changes in rainfall erosivity in the US with climate change during the 21st century. *Journal of Soil and Water Conservation*, 56(3), pp.229–232.

Nicks, A.D. & Gander, G.A., 1994. CLIGEN: a weather generator for climate inputs to water resource and other models. In *Proc. Fifth Int. Conf. on Computers in Agriculture*. pp. 903–909.

Nissan, H. & Toumi, R., 2013a. Dynamic simulation of rainfall kinetic energy flux in a cloud resolving model. *Geophysical Research Letters*, 40(12), pp.3331–3336.

Nissan, H. & Toumi, R., 2013b. On the impact of aerosols on soil erosion. *Geophysical Research Letters*, 40, pp.5994–5998.

Pimentel, D. et al., 1995. Environmental and economic costs of soil erosion and conservation benefits. *Science*, 267, pp.1117–1123.

Pruski, F.F. & Nearing, M.A., 2002a. Climate-induced changes in erosion during the 21st century for eight U.S. locations. *Water Resources Research*, 38(12), pp.34–1–34–11. Available at: http://doi.wiley.com/10.1029/2001WR000493 [Accessed October 4, 2013].

Pruski, F.F. & Nearing, M.A., 2002b. Runoff and soil-loss responses to changes in precipitation: A computer simulation study. *Journal of Soil and Water Conservation*, 57(1), pp.7–16.

Ramanathan, V. et al., 2005. Atmospheric brown clouds: impacts on South Asian climate and hydrological cycle. *Proceedings of the National Academy of Sciences of the United States of America*, 102(15), pp.5326–5333.

Renard, K.G. et al., 1997. *Predicting soil erosion by water: a guide to conservation planning with the Revised Universal Soil Loss Equation (RUSLE)*,

Renard, K.G. & Freimund, J.R., 1994. Using monthly precipitation data to estimate the R-factor in the revised USLE. *Journal of Hydrology*, 157, pp.287–306.

Singh, G. et al., 1992. Soil erosion rates in India. *Journal of Soil and Water Conservation*, 47(1), pp.97–99.

Skamarock, W.C. et al., 2008. A Description of the Advanced Research WRF Version 3. *NCAR Technical Note NCAR/TN-475+STR*, (June).

Squires, P. & Twomey, S., 1960. The relation between cloud droplet spectra and the spectrum of cloud nuclei. In *Physics of Precipitation: Proceedings of the Cloud Physics Conference, Woods Hole, Massachusetts, June 3-5, 1959*. pp. 211–219.

Srinivas, C. V. et al., 2013. Simulation of the Indian summer monsoon regional climate using advanced research WRF model. *International Journal of Climatology*, 33(5), pp.1195–1210. Available at: http://doi.wiley.com/10.1002/joc.3505 [Accessed April 28, 2014].

Thompson, G. & Eidhammer, T., 2014. A Study of Aerosol Impacts on Clouds and Precipitation Development in a Large Winter Cyclone. *Journal of the Atmospheric Sciences*, 71(10), pp.3636–3658. Available at: http://journals.ametsoc.org/doi/abs/10.1175/JAS-D-13-0305.1 [Accessed February 25, 2015].

Turner, A.G. & Annamalai, H., 2012. Climate change and the South Asian summer monsoon. *Nature Climate Change*, 2(June).

UNEP, 2007. Chapter 3: Land. In *Global Environment Outlook-4: Environment for development (GEO-4)*. Malta.

Wischmeier, W.H. & Smith, D.D., 1978. *Predicting rainfall erosion losses: a guide to conservation planning*,

Wischmeier, W.H. & Smith, D.D., 1958. Rainfall energy and its relationship to soil loss.

Transactions, American Geophysical Union, 39(2), pp.285–291.

Yang, D. et al., 2003. Global potential soil erosion with reference to land use and climate changes. *Hydrological Processes*, 17(14), pp.2913–2928.

Zhang, X.-C., 2007. A comparison of explicit and implicit spatial downscaling of GCM output for soil erosion and crop production assessments. *Climatic Change*, 84(3-4), pp.337–363. Available at: http://link.springer.com/10.1007/s10584-007-9256-1 [Accessed October 25, 2013].

Zhang, X.-C., 2005. Spatial downscaling of global climate model output for site-specific assessment of crop production and soil erosion. *Agricultural and Forest Meteorology*, 135(1-4), pp.215–229. Available at: http://linkinghub.elsevier.com/retrieve/pii/S0168192305002534 [Accessed October 25, 2013].

Zhang, Y.-G. et al., 2010. Projected rainfall erosivity changes under climate change from multimodel and multiscenario projections in Northeast China. *Journal of Hydrology*, 384(1), pp.97–106.

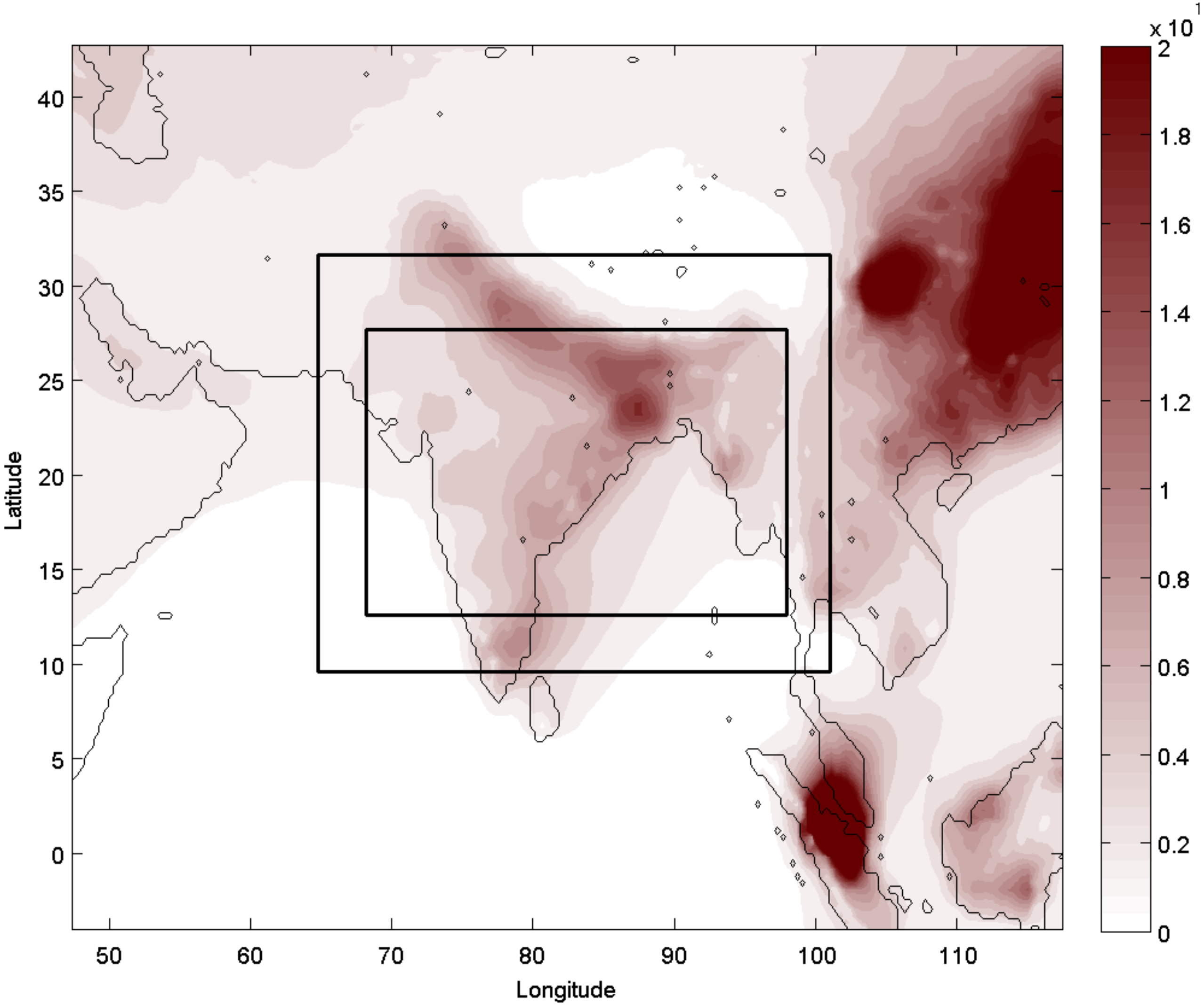

x 10^10
2
1.8
1.6
1.4
1.2
1
0.8
0.6
0.4
0.2
0
40
35
30
25
20
15
10
5
0
Latitude
50
60
70
80
90
100
110
Longitude


a)
b)
c)
Latitude
Longitude
0
5
10
15
20
25
30

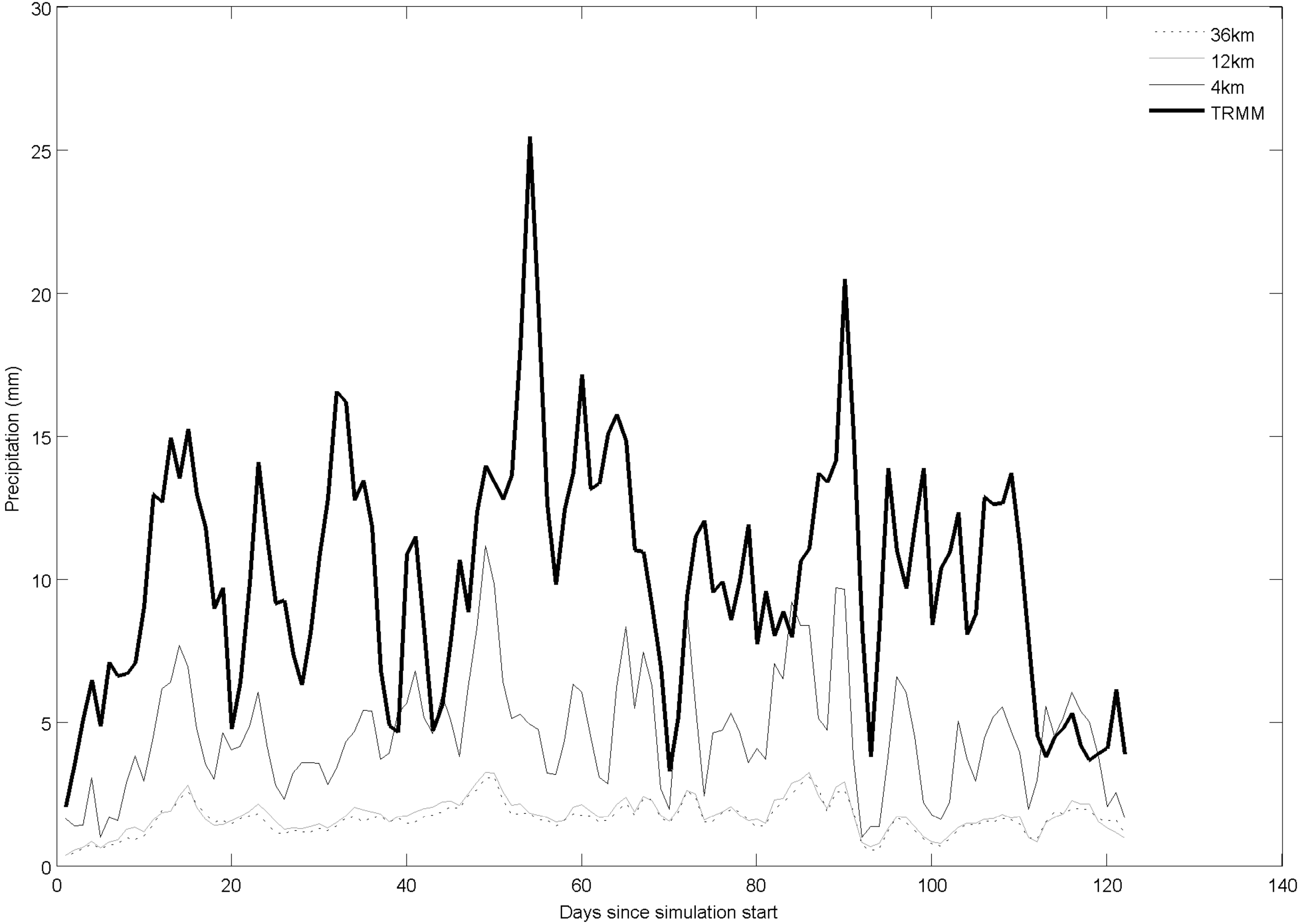
36km
12km
4km
TRMM
Precipitation (mm)
Days since simulation start
0
5
10
15
20
25
30
0
20
40
60
80
100
120
140

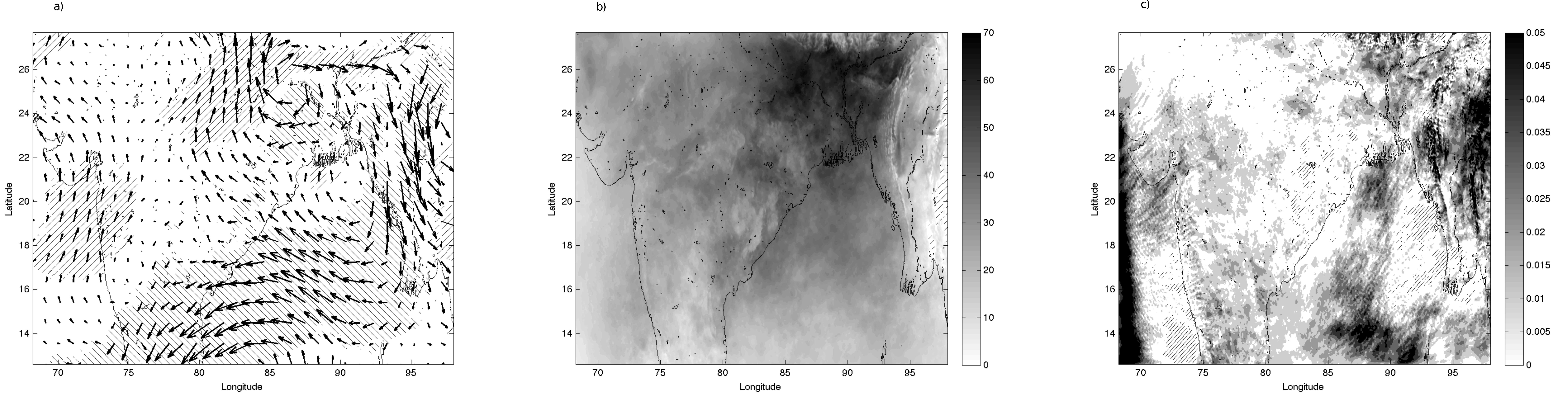

a)
b)
c)
Latitude
Longitude
26
24
22
20
18
16
14
70
75
80
85
90
95
70
60
50
40
30
20
10
0
0.05
0.045
0.04
0.035
0.03
0.025
0.02
0.015
0.01
0.005
0

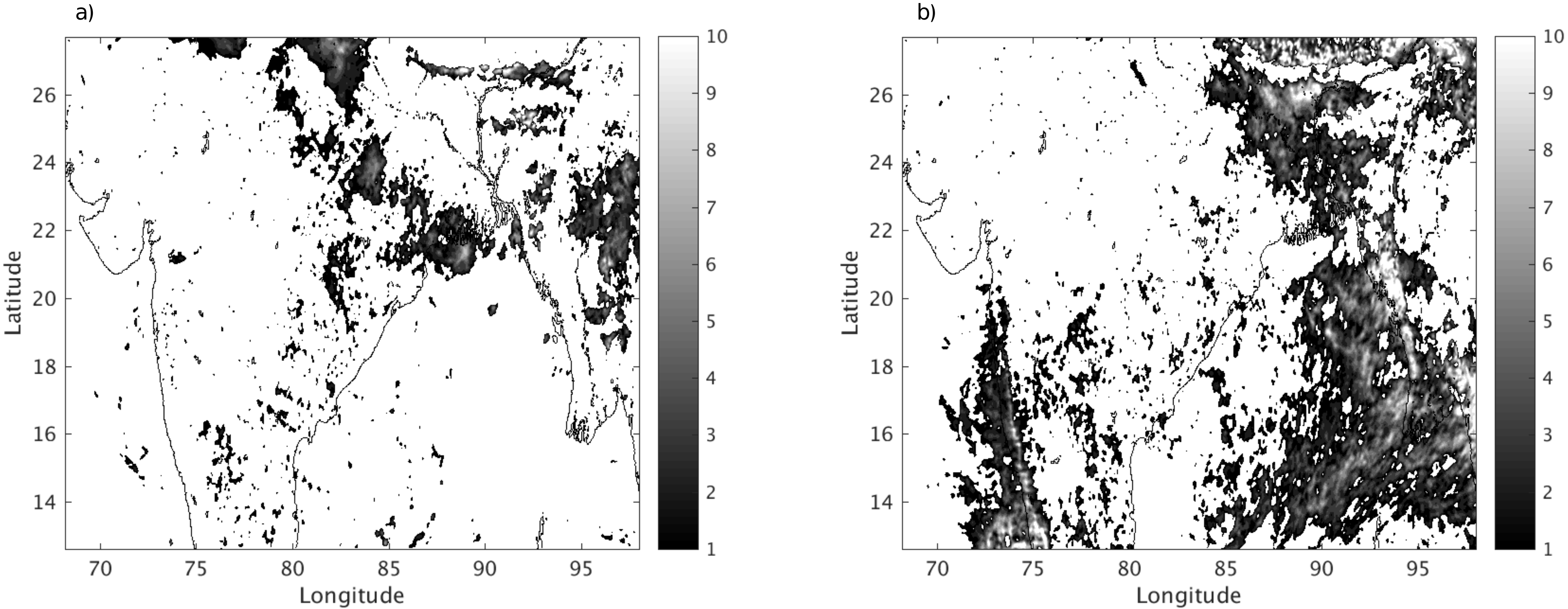

a)
b)
Latitude
Longitude
26
24
22
20
18
16
14
70
75
80
85
90
95
10
9
8
7
6
5
4
3
2
1

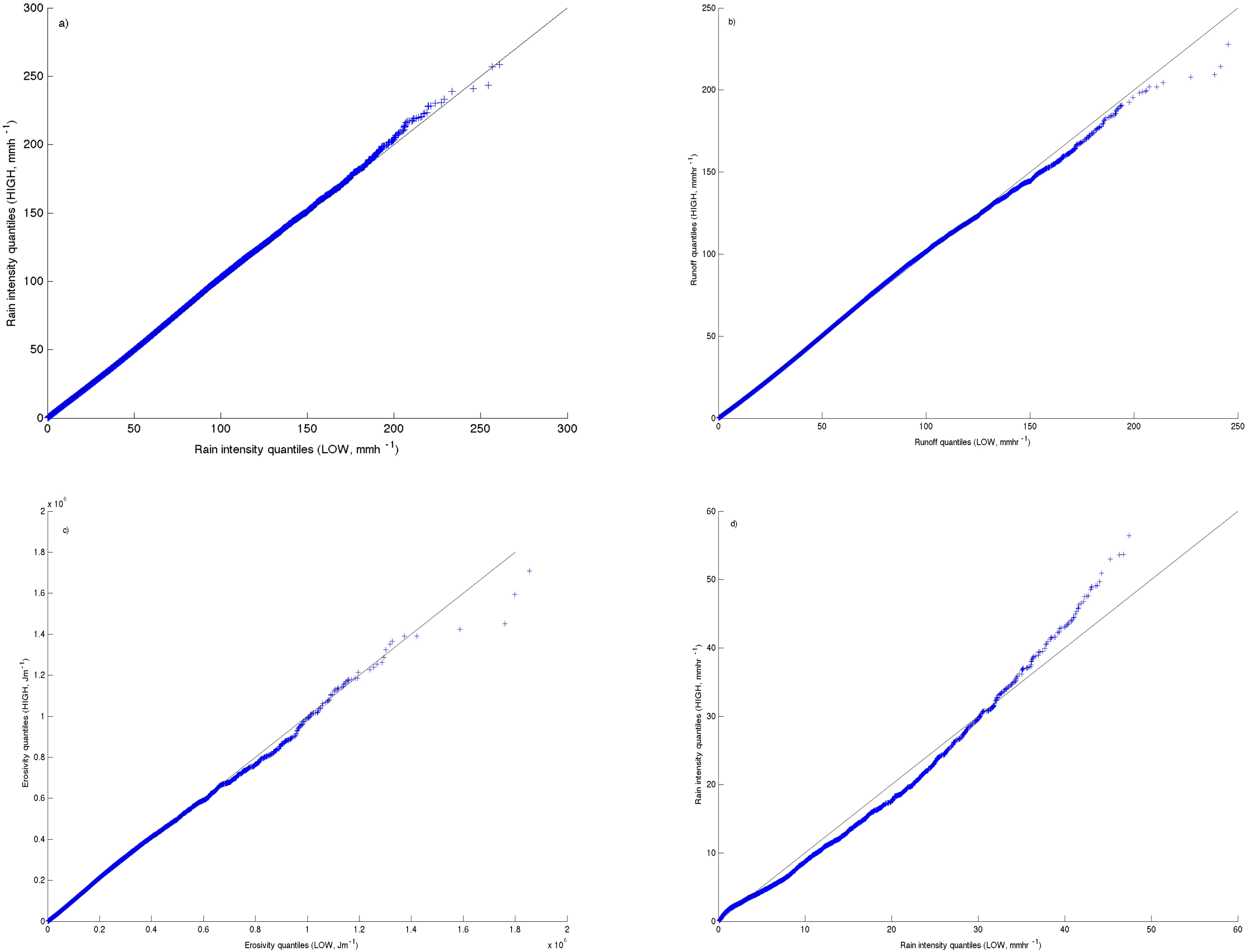
a)
Rain intensity quantiles (HIGH, mmh -1)
Rain intensity quantiles (LOW, mmh -1)
0
50
100
150
200
250
300
b)
Runoff quantiles (HIGH, mmhr -1)
Runoff quantiles (LOW, mmhr -1)
0
50
100
150
200
250
c)
x 10^6
Erosivity quantiles (HIGH, Jm-1)
Erosivity quantiles (LOW, Jm-1)
x 10^6
0
0.2
0.4
0.6
0.8
1
1.2
1.4
1.6
1.8
2
d)
Rain intensity quantiles (HIGH, mmhr -1)
Rain intensity quantiles (LOW, mmhr -1)
0
10
20
30
40
50
60

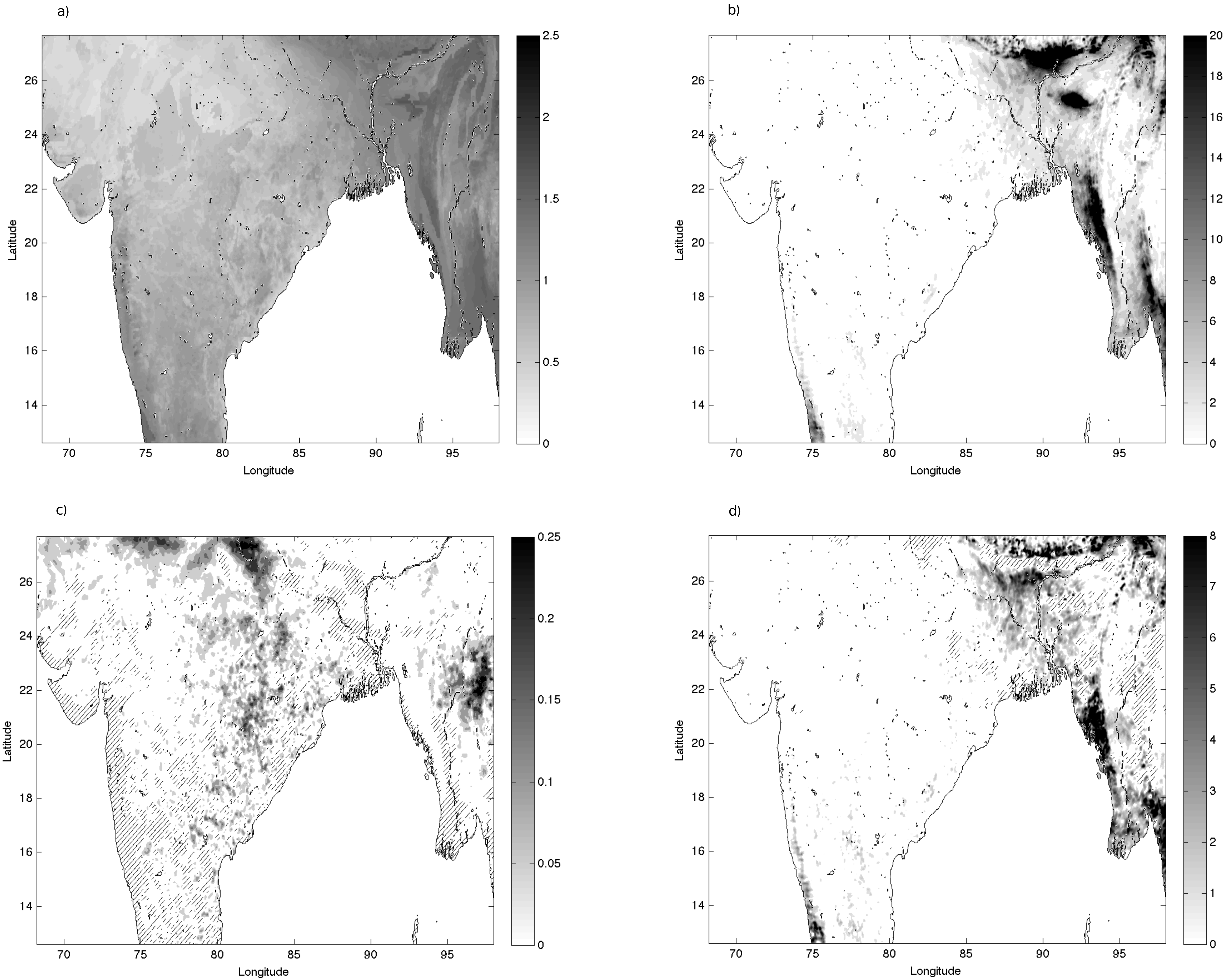
a)
b)
c)
d)
Latitude
Longitude
26
24
22
20
18
16
14
70
75
80
85
90
95
2.5
2
1.5
1
0.5
0
20
18
16
14
12
10
8
6
4
2
0
0.25
0.2
0.15
0.1
0.05
0
8
7
6
5
4
3
2
1
0

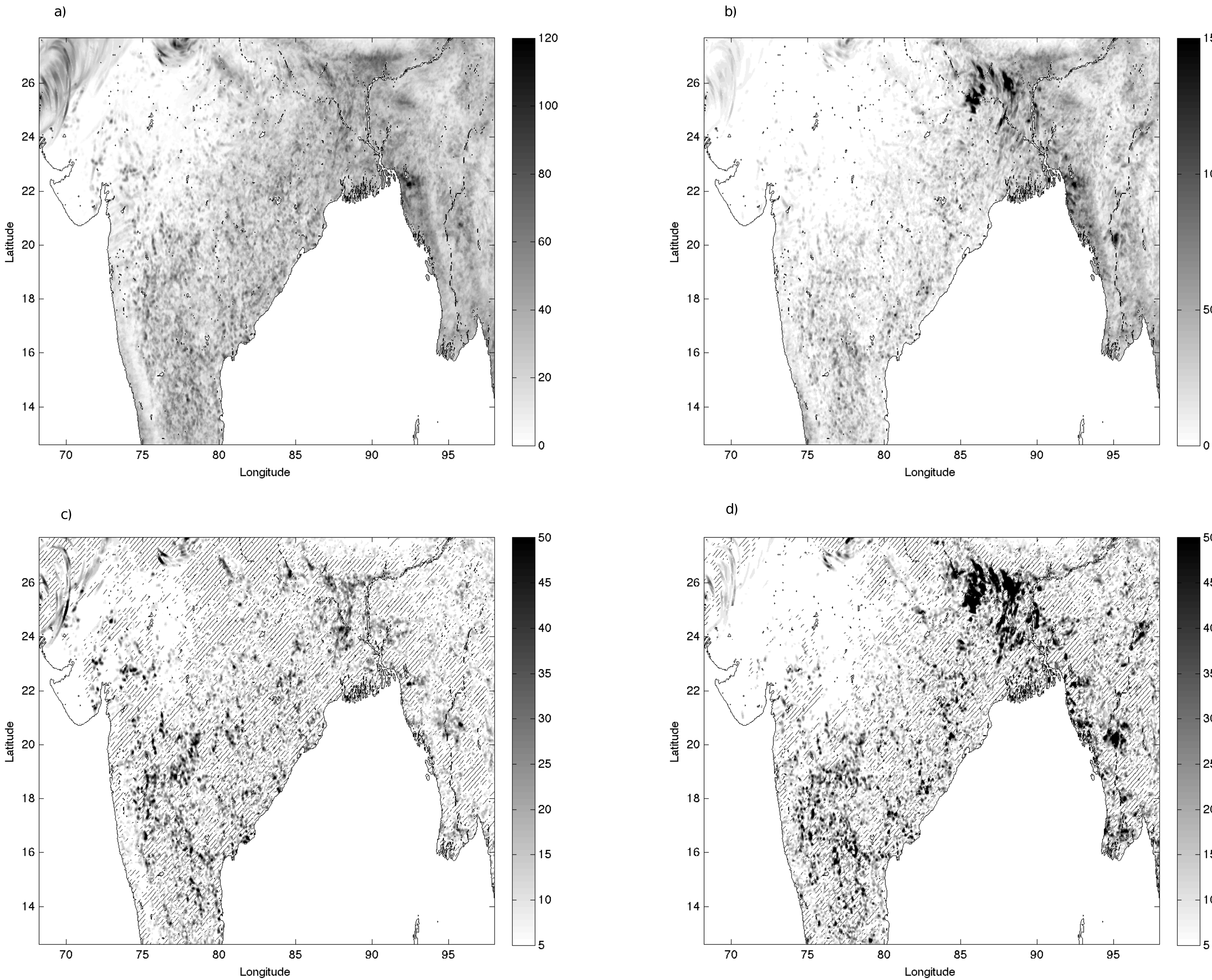

a)
b)
c)
d)
Latitude
Longitude

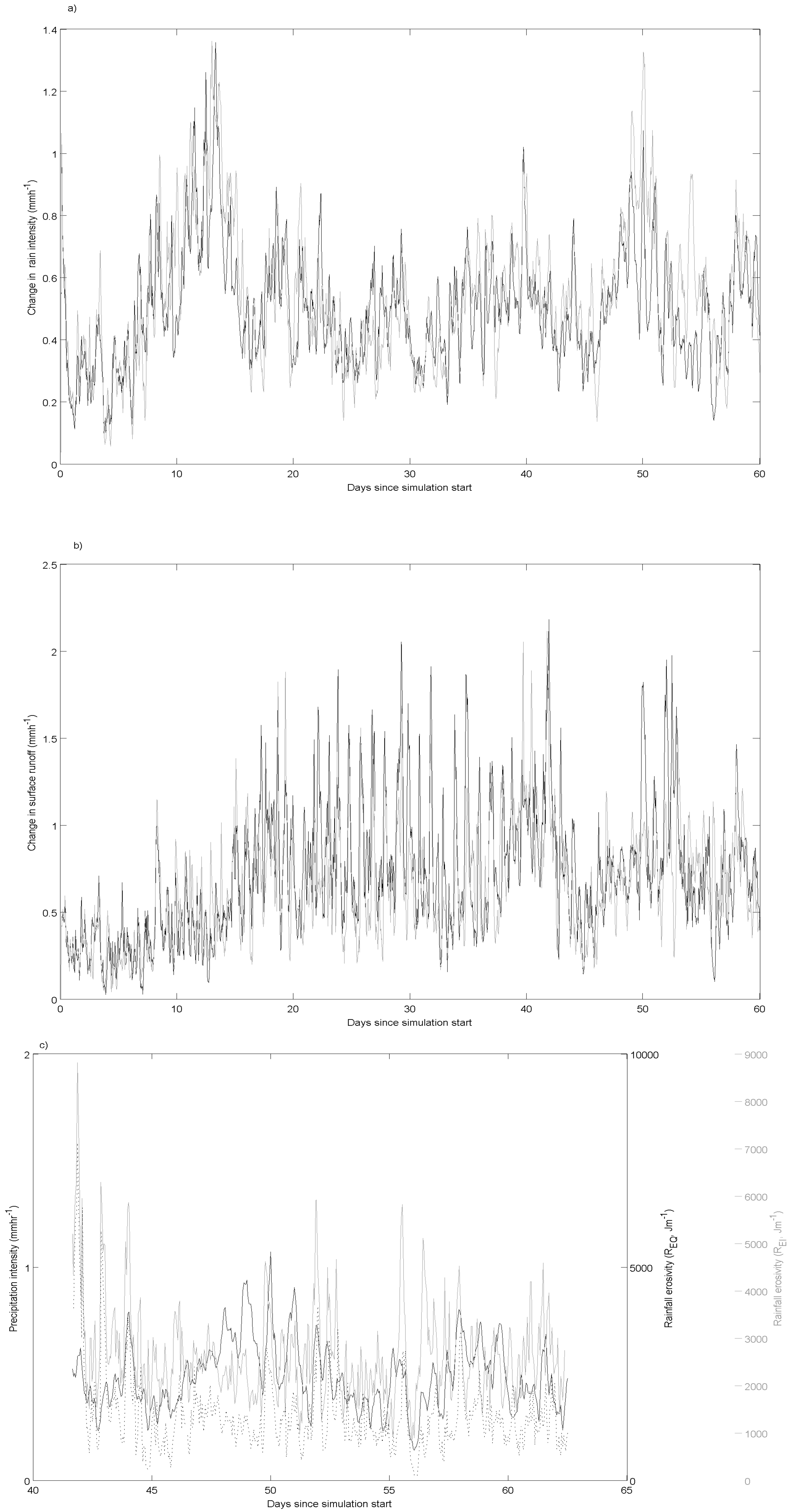

a)
Change in rain intensity (mmh-1)
Days since simulation start
b)
Change in surface runoff (mmh-1)
Days since simulation start
c)
Precipitation intensity (mmhr-1)
Rainfall erosivity (REQ, Jm-1)
Rainfall erosivity (REI, Jm-1)
Days since simulation start

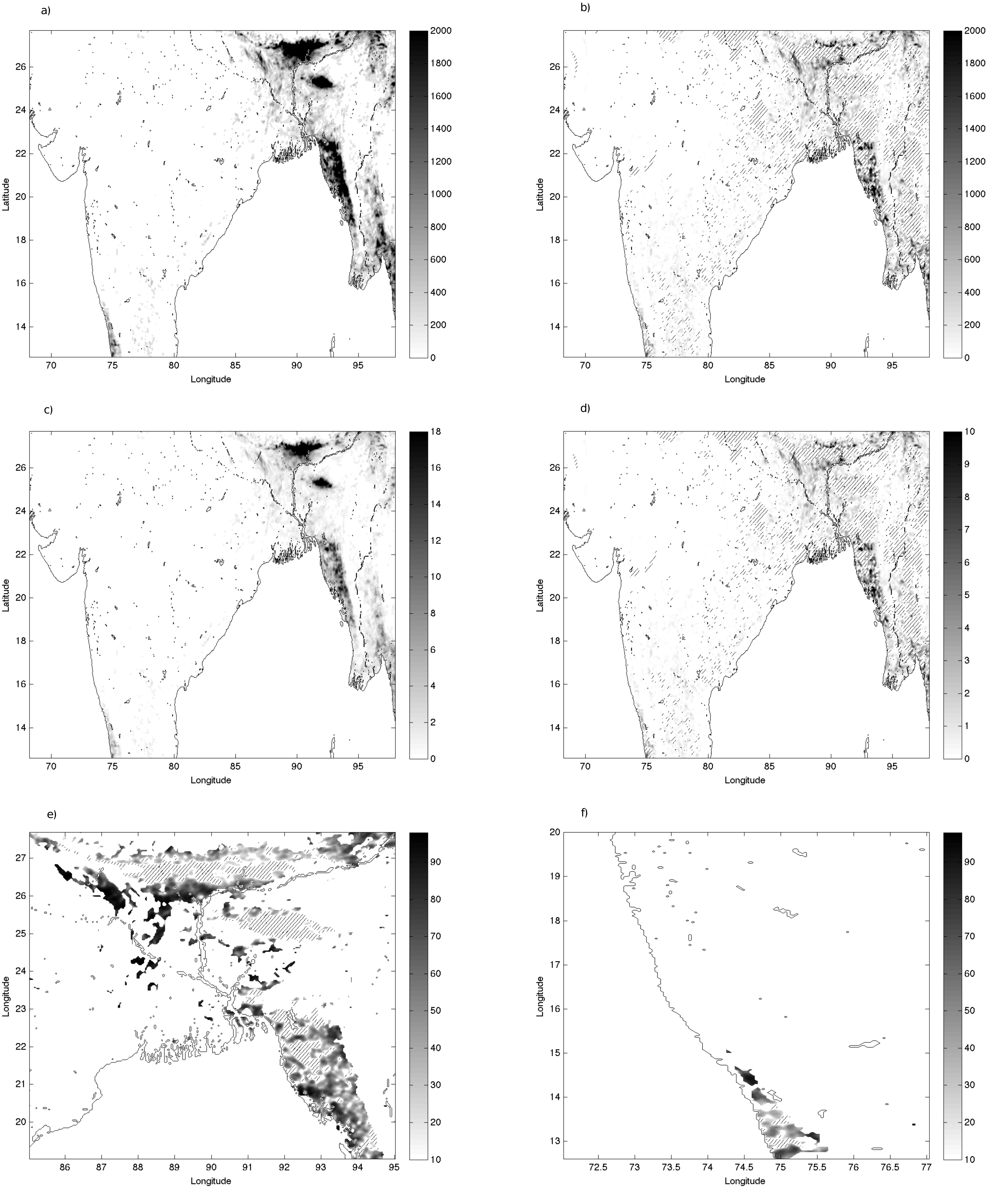

a)
b)
c)
d)
e)
f)
Latitude
Longitude